Aerosol-Jet Printed Fine-Featured Triboelectric Sensors for Motion Sensing

*Qingshen Jing, Yeon Sik Choi, Michael Smith, Nordin Catic, Canlin Ou, Sohini Kar-Narayan**

Dr Q. Jing, Y. S. Choi, M. Smith, N. Catic, C. Ou, Dr S. Kar-Narayan

Department of Material Science & Metallurgy, University of Cambridge, CB3 0FS, UK

E-mail: sk568@cam.ac.uk

Keywords: aerosol-jet printing, triboelectricity, motion sensor

Abstract

Triboelectric motion sensors, based on the generation of a voltage across two dissimilar materials sliding across each other as a result of the triboelectric effect, have generated interest due to the relative simplicity of the typical grated device structures and materials required. However, these sensors are often limited by poor spatial and/or temporal resolution of motion due to limitations in achieving the required device feature sizes through conventional lithography or printing techniques. Furthermore, the reliance on metallic components that are relatively straightforward to pattern into fine features limits the possibility to develop transparent sensors. Polymers would allow for transparent devices, but these materials are significantly more difficult to pattern into fine features when compared to metals. Here, we use an aerosol-jet printing (AJP) technique to develop triboelectric sensors using a wide variety of materials, including polymers, which can be directly printed into finely featured grated structures for enhanced sensitivity to displacement and speed of motion. We present a detailed investigation highlighting the role of material selection and feature size in determining the overall resolution of the resulting motion sensor. A 3-channel rotary sensor is also presented, demonstrating the versatility of the AJP technique in developing more complex triboelectric motion sensors.

Introduction

Motion sensing, or the ability to resolve displacement, direction and velocity, is essential in applications related to manufacturing, mapping, transportation, as well as emerging fields such as robotics and personalised medicine. Current technologies for sensing applications in these areas are mostly based on electromagnetic interaction[1–5], optical sensing[6,7], potentiometry[8], and capacitive devices[9,10]. Although well-developed, these technologies suffer from limitations such as being power-dependent, bulky, rigid, and non-transparent. More recently, triboelectric generators[11] have been widely investigated for designing self-powered motion sensors[12–14] due to the relatively simple mechanism involved in converting mechanical energy into electrical signals[15,16], wide material selection[17,18] and light weight[19]. Triboelectric generators produce active electric output due to mechanical motion-driven contact electrification and charge induction. These generators can also be used as sensors, where the output signal can be monitored for sensing movement [20–24]. One particular type of triboelectric sensor designed for motion sensing, based on grated electrode structures on triboelectric surfaces, has been found to be potentially reliable, high-resolution and direction-sensitive with a wide selection of feasible materials[25,26]. Typically, these sensors comprise of multiple alternating strips of two different triboelectric materials for contact electrification, and grated comb-like electrodes or interdigitated electrodes for charge induction. A commonly reported device structure involves a "mover" which slides over a "stator", with the contacting surface made up of triboelectric material strips, and the grated electrodes positioned on the backside of both the mover and the stator to form a sliding mode triboelectric sensor[21]. The relative sliding motion between the two different materials gives rise to a triboelectric charge that is picked up by the electrodes. If the electrodes are positioned only on the backside of the stator, then this structure gives rise to a freestanding mode triboelectric sensor (no electrical contact is needed from the mover)[27]. To achieve high resolution, the metallic electrode gratings must be narrow (sub-millimetre), usually achieved via photo-lithography[28], physical deposition[26,29] or ion-etching[30] methods. These methods are not particularly cost-effective and are generally inefficient for fast prototyping. At the same time, polymers which have good triboelectric properties are difficult to fabricate into the desired fine structures or finely patterned strips

by conventional lithography or physical deposition methods. This has led to the vast majority of the current grated-structure triboelectric sensors being built with metal strips as the active triboelectric material[31,32], even though these are not particularly well-suited for triboelectric applications. Reports on all-polymer grated triboelectric sensors are thus tellingly rare, even though such devices could potentially offer better resolution and higher signal-to-noise ratios in motion sensing applications.

Here, we adopt an aerosol-jet printing (AJP) technique to develop novel triboelectric sensors by the direct and rapid printing of both metallic and polymeric inks into the desired finely grated structures for high-resolution motion sensing. AJP is a high-resolution rapid-prototyping facility that is compatible with a broad selection of inks with a wide range of viscosities[33–35]. Inks are atomized by either pneumatic or ultrasonic excitation into micron-sized aerosol droplets, which are carried in a nitrogen carrier gas to the printer nozzle, and focused into the desired size by the use of a sheath gas, such as nitrogen (as shown in Supplementary Figure S1). A variety of compatible inks including those based on metallic and ceramic nanoparticles[34,35], carbon nanotubes[36], polymers[35] and polymeric precursors[37], with ink viscosities from 1 cP to 1000 cP can be directly printed with minimum feature size a small as 10 μm[34]. AJP benefits from the ability to rapidly print customized patterns, as well as large working space (up to 175 mm × 200 mm in the Optomec AJ200 printer used in this work), making it a powerful tool for fabricating triboelectric nanogenerators in a scalable way. Its ability to print polymeric materials at micrometre resolution also helps study performance of triboelectric sensors with control over device design and material selection. Taking advantage of this versatile technique, we first printed a metal-polymer grated-structure triboelectric motion sensor with a strip width of 25 μm, resulting in a spatial resolution down to 50 μm. The sensor gave rise to reliable output voltage signals in response to slow sliding speeds ranging from 50 μm/s to 300 μm/s. Further tests on multiple combinations of material selections for gratings, including polymer-polymer gratings, were conducted using the AJP technique, in order to compare their performance. The metallic electrodes for charge induction could be either directly printed by AJP, or in an indirect way by first printing a mask followed by physical deposition of the metal, depending on which was more effective for achieving the specific device design. Furthermore, making use of the rapid prototyping ability afforded by AJP, we also

designed and fabricated a three-channel triboelectric "rotary" sensor for angular and directional detection with enhanced reliability as compared to a previously reported prototype[25]. Our proposed method to develop triboelectric motion sensors via AJP can be easily adapted to produce high-resolution fast prototypes, based on a wide range of materials, as well as large-scale fabrication capability that is desirable for commercialisation.

Ultra-fine grated-pattern triboelectric motion sensor

There have been quite a few successful attempts at utilizing grated-structure triboelectric generators as active motion sensors[15,20,25]. However, the ultimate resolution of such sensors highly depends on how narrow the grating can be made. As an example, a triboelectric generator developed using micro-fabrication approaches including photolithography and vapor deposition, that had a 200 μm grating period was reported to achieve sub-micrometer resolution in displacement sensing[28]. Apart from the complex processing steps, the design of this micro triboelectric sensor requires wired connections to both moving and static parts, which is not desirable for motion sensors. Freestanding type of triboelectric generators[27] and sensors[26], which contain no wire connections on the movers but instead have interdigitated electrodes on the stators, have been shown to overcome this problem, as illustrated in Figure 1a. However, other problems emerged when attempting to make the period of the grating smaller for better motion sensing resolution, as this required good separation between the electrode strips to prevent unintentional short circuits. Previous work in this area[25] showed that depositing grated electrodes on opposite sides of a polymer film could resolve the issue by making use of the polymer itself for electrical insulation. However, as the width of the strips is reduced, conventional micro-fabrication methods which require separate deposition procedures for each side are less effective due to the difficulty in aligning the two branches of the interdigitated electrodes on either side of the polymer film.

In this work, we have fabricated an ultra-fine grated and patterned interdigitated electrode structure by printing silver and polyimide inks onto flexible polyimide substrates, which make up the main functional parts for the mover and the stator of the sensor. For the stator (Figure 1c) which contained a pair of interdigitated electrodes at a period of 50 μm, the fabrication process started with

first printing finely grated “comb” electrode structures on the polyimide substrates using Ag nanoparticle ink. This is followed by printing an insulating layer from polyimide ink, and a second grated comb electrode structure from Ag ink on the top (as shown in Figure 1d). The centres of the comb electrodes on either side are displaced by half a pitch to form a pair of interdigitated electrodes. For the mover, a grated pattern with a period of 100 μm was printed on polyimide film with Ag ink (Figure 1b). The cross-section of the stator is shown in Figure 1e. The image clearly shows that by printing a thin layer of polyimide in between the electrodes, the interdigitated electrode pairs were well isolated with minimum horizontal separation. This process was adopted with the aim of achieving the minimum grating resolution for the interdigitated electrode pairs as could be afforded by the AJP technique. The electrodes on the stator and the pattern on the mover possessed total area of about 200 mm^2 and 40 mm^2, respectively. The working mechanism of this triboelectric sensor operating in free-standing mode is depicted in Supplementary Figure S2, where the dynamic flow of electrons between the interdigitated electrodes on the stator is shown to be induced by the triboelectric charge generated as a result of the relative motion between the stator and mover. Importantly, in our design, the electrodes are printed on the back of the contacting surface of the stator, separated by a dielectric layer to prevent shorting. The printed electrodes therefore do not directly make contact with the mover, and are thus well-protected from the effects of friction (Figure 1a, Figure S2).

The fully printed triboelectric sensor was then mounted onto a linear motor (LinMot), with the mover attached to the motor arm with a piece of sponge for conformal contact, and the stator fixed on the base (Figure 1f). Driven by different speeds ranging from 50 μm/s to 300 μm/s, the normalized open-circuit voltage (V_{oc}) signals measured across the interdigitated electrodes on the stator are shown in Figure 1g. All V_{oc} generated showed amplitudes around 20~25 mV, regardless of the speeds, which was consistent with triboelectric generator performance reported before[38,39]. The periods of the signals, however, were distinct and consistent with the sliding speed, meaning a continuous monitoring of V_{oc} could sense the sliding distance and speed of the mover. However, noticeable measuring errors occurred in measured signals at all speeds, for example, a single period of the signal at 50 μm/s sliding speed should have corresponded to a 1 s time span, but instead corresponded to ~ 1.3 s. Given the fact that

these errors consistently appeared in the measured data on a similar scale, we believe that these are therefore likely to be systematic errors related to the installation of the mover and stator, such as relaxation of the sponge or shift of the film with electrodes. The errors can be therefore eliminated by normalization or calibration of the signal using more accurate actuators, to achieve higher reliability and accuracy as desired in a micrometre-level active motion sensor. Furthermore, higher sliding speeds can be recorded by increasing the sampling rate of the measurement system. Overall, the device showed reasonably stable output over thousands of sliding cycles, as shown in Supplementary Figure S3.

Since the magnitude of V_{oc} was hardly influenced by the sliding speed, the signal could be normalized by multiplying time with speed, resulting in a conversion of the *x*-axis from time (s) to distance (μm) (Figure 1h). The gradient of the curve in Figure 1h indicates a sensitivity of up to around 630 μV/μm, showing the sensor's ability to measure displacements with micrometer, or even sub-micrometer, resolution. Compared with previous work on nanometre resolution triboelectric sensors[28], our sensor showed lower voltage sensitivity per unit-displacement. Simulations based on finite element analysis (FEA) were conducted with regards to this situation, with results shown in Supplementary Figure S4. The results of FEA simulations investigating the printed grating width support the observation that V_{oc} is strongly dependent on the width of the gratings (Figure S4 c). Significantly narrower grated electrodes enable the edge effect and charge leakage effect to become more dominant. However, another factor that may influence the output magnitude is the degree of alignment between stripes on the mover and electrodes on the stator. Simulation results in Supplementary Figure S4 d show that as the width of the electrode stripes decreases, the V_{oc} amplitude decreases more dramatically at smaller angular mismatches. In our experiments, the alignments were mostly done by visual inspection, aided by real-time monitored V_{oc} values to pinpoint the alignment from which the largest output resulted. We believe therefore that there is still room for the signal amplitude to be improved through optimised experimental set-ups.

Material selections for grated-structure sliding-mode triboelectric sensors

Metals such as copper and aluminum are relatively easily deposited into thin strips on polymer substrates to form metal-polymer paired triboelectric generators, and thus these have been widely

reported in generators with finely grated structures[15,25]. Although emphasis has been laid on material selection as being critical in designing triboelectric generators[17,40], there have been relatively few studies comparing the performance of different triboelectric materials in grated-structure-type generators or sensors. This has been due to lack of a consistent and fast-prototyping technique for the fabrication of polymer-polymer grated-structure sliding generators, as compared to the more commonly studied metal-polymer ones. With AJP however, it is possible to fabricate fine-featured polymer structures with feature width as small as that achieved using metals, which makes it an ideal tool for study material-dependent output of grated-structure based sliding generators.

Three different inks - Ag nanoparticle, polyimide (Kapton) and PVDF-TrFE (polyvinylidene difluoride-trifluoroethylene) - were printed as stripes on selected substrates with a period of 600 μm, forming movers with different combination of materials including: Ag on Kapton, PVDF-TrFE on Kapton, Kapton on Nylon, Kapton on Teflon and Kapton on Aluminium foil (Figure 2a). The movers were respectively driven by the linear motor over a stator containing interdigitated electrodes covered with Kapton film fabricated via the direct printing method. With a sliding speed of 1 mm/s, normalized open-circuit voltages from different types of movers are compared in Figure 2b. From our experiment, movers with all pairs of materials showed periodic signals that were consistent with sliding speed. Interestingly, the highest V_{oc} was acquired from the Ag-Kapton pair, which was higher than Kapton-Nylon, even though the latter pairing was expected to generate a larger amount of charge transfer considering the relative positions of the respective materials on the triboelectric series[17]. We believe this conflicting behavior is due to variation in surface smoothness of the printed materials, where with respect to Kapton (polyimide), the surface of the printed silver gratings had a rougher surface compared with the surface of the Nylon film (Supplementary Figure S5). It has been reported that higher roughness of the contacting surface is likely to induce more charge transfer due to larger surface area[17]. However, polymer-based movers such as Kapton on Nylon and PVDF-TrFE on Kapton have the unique advantage of being transparent and flexible compared to devices containing metallic components. This can be advantageous for motion sensors especially when these are used in conjunction with optical or visual

surfaces, such as panels or display screens. Also, being flexible means that the sensor can in principle be attached to curved surfaces.

AJP-assisted dry-etching approach for large-scale interdigitated electrode fabrication

Although AJP is well-suited for fabricating fine interdigitated electrodes for triboelectric motion sensors, there are some situations when sensors may need a wider design of grated electrodes. For example, for a faster range of motion monitoring, motion sensors with wider electrodes can be useful to generate a signal frequency comparable with that from narrower electrodes at lower speed, so that the sampling rate limitation from a given data collection module would not be a handicap for signal processing (detailed calculations are presented in Supplementary Note S1). Direct printing of wider electrodes requires rastering over a certain area, which can be time-consuming considering the relatively small dimensions of the AJP features, with a maximum feature size being around 150 μm to 200 μm as printed from a 300 μm wide tip. Alternatively, an AJP-assisted "dry-etching" approach has been introduced to speed-up the process. The approach involved mask printing, metal deposition, and mask dry-removal. As an example, a wide gold interdigitated electrode structure fabricated on the glass substrate was demonstrated. A thermoplastic polyurethane (PU) ink was used to print a suitable "mask" due to its relatively large tensile strength in relation to its stretchability (Supplementary Table S1), as well as its reasonably low adhesion with glass. To create an interdigitated electrode, the mask pattern was designed to be a serpentine path, as shown in Figure 2c. The intersection features of the PU lines are 250 μm wide and 50 μm high as shown by surface profilometer measurements (Figure 2d). After being dried in air at 80 ˚C for 15 min, the masked glass was sputtered with a layer of gold with a thickness of about 200 nm (Figure 2e). The PU was then removed by simply peeling it off from the glass substrate (Figure 2f, Supporting Video), leaving a neat, well-separated wide interdigitated electrode structure (Figure 2g, 2h). Further tests showed that PU could also be applied onto various soft substrates for easy peel-off, including Nylon, Teflon and aluminium foil. The PU mask could not be applied onto Kapton, however, due to strong bonding force between the two polymer molecules which makes the dry-etching lift-off difficult. Alternatively, inks such as PVDF could be used for printing the

mask on Kapton, however this would require a wet-etching method, such as washing in acetone, to remove.

AJP-printed motion sensor based on 3-channeled triboelectric signals.

Single-channel grated-structure triboelectric sensors have been shown to be capable of monitoring motion speed[26], while double-channeled sensors have been studied to realize directional motion detection[25]. The mechanism for double-channeled triboelectric sensor to detect motion direction is based on timing the signals' phase difference, which can be unreliable in certain moving configurations such as irregular accelerations/decelerations (Supplementary Figure S6). Moreover, the 2nd channel which provides the reference signal does not help to increase the detecting resolution due to its structural design of an asymmetric space shift compared with the main channel[25].

To increase the reliability as well as resolution, a new design of directional rotary motion sensor containing three channels of active signals is fabricated by AJP. The sensor is composed of two parts (Figure 3a): the mover comprising a three-channel array of concentrically radial, grated-structure polyimide printed on Nylon film (Figure 3b), and the stator comprising a three-channel array of concentric interdigitated silver electrodes printed on Kapton film (Figure 3c). Grating segments from all channels on the stator were aligned radially. Each channel contained 45 pairs of electrode segments, resulting in an 8˚ resolution per single channel (Figure 3c, 3e). Accordingly, there are 45 segments of polyimide in each channel on the mover. Segments from one channel possessed a ± 1/3 period shift against the remaining two channels (Figure 3b, 3d), resulting in asynchronous signals between channels generated by sliding rotation between the mover and the stator. Figure 3d & 3e also show the designed printing path to fill up the pattern for each channel. Benefiting from this unique design, when three channels of signals are monitored simultaneously and compared, the angular resolution was found to increase by up to 3 times compared to any single channel. The signal processing module includes a microcontroller unit (MCU) that simultaneously monitored the three channels of triboelectric output over external loads (Figure 4a). In our situation we used 20 MΩ resistors as R_2 for each channel. Analog signals from each channel were tagged (coloured in Figure 4b) and compared by their sequence (see Supplementary Note S2 for details). In a clockwise rotatory sensing situation (Figure 4c), the emergence

of upward peaks resulted in order from channel 1 through to channel 3. In contrast, this order reversed from channel 3 to channel 1 in response to a counter-clockwise rotation (Figure 4d). Thus, rotary direction can be simply determined by checking the sequence of the channel tag numbers in the order of appearance of their signal peaks, while the rotated angle presented between adjacent peaks is simply the shifting angle between different channels, which is 8/3rd of a degree in our prototype. This information was then collected and processed by the MCU to calculate the absolute angular position for the sensor. A practical demonstration is shown in the supplementary movie, presenting a reliable angular measurement in both rotating directions. Improvement in the sensor performance can be achieved by implementing better algorithms for the signal processing, including taking into account the negative peaks in the output which could double the angular resolution.

Conclusions

Various approaches to fabricate self-powered triboelectric sensors based on AJP have been demonstrated and studied. The fine-featured pattern generated from AJP helps to create an ultra-fine grated-structure triboelectric motion sensor that can achieve a reliable spatial resolution of up to 50 μm, at a speed detection level of micrometers per second. Meanwhile, the excellent compatibility of a variety of inks with the AJP process enables the study of polymer-polymer grated structures as active triboelectric surfaces for motion sensors, which signals a departure from metallic gratings commonly used in these types of devices, and could further lead to the development of transparent and flexible triboelectric sensors. Strategies for larger dimension, large-scale interdigitated electrode fabrication assisted by the AJP by printing process has also been demonstrated. A fully printed, three-channel rotary triboelectric sensor is presented using AJP. By sharing 1/3 phase difference between each channel, the sensor could reliably indicate the rotating angle as well as direction, at high resolution. All these prototypes also benefit from being transparent and flexible as thin films. AJP has therefore been shown to enable high resolution, fast prototyping speed, wide material adaptation, and large-scale fabrication required for wide-ranging triboelectric sensor applications.

Methods

Making and printing of Ag ink

0.6 ml of silver nanoparticle ink (PRELECT® TPS 50 Nano Ag ink) was mixed with DI water at 1:1 ration to form 1.2 ml of silver ink. The ink was then placed in the glass vial for the ultrasonic atomizer of an Optomec AJ200 aerosol jet printer. A 150 μm sized nozzle was used. A flow rate of 30 standard cubic centimetres per minute (sccm) N_2 carrier gas and a sheath flow rate of 55 sccm were adopted to achieve a line feature of ~25 μm. The printed silver pattern was annealed at 150 ˚C for 12 hours or 200 ˚C for 3 hours, depending on the properties of the substrates.

Making and printing of PVDF-TrFE ink

PVDF-TrFE (70/30 weight%, Piezotech) was dissolved in N-Methyl-2-pyrrolidone (NMP, Sigma-Aldrich) at 4 wt% under constant stirring at 60 °C. Around 20 ml of the PVDF-TrFE ink was placed in the bottle for the pneumatic atomizer. A 250 μm sized nozzle was used. An atomising flow rate of 1100 sccm, an exhaust rate ratio of 950 sccm and a sheath flow rate of 140 sccm were adopted. Samples were dried at 130 ˚C for 2 hours.

Making and printing of polyimide ink

Polyamic acid (Poly(pyromellitic dianhydride-co-4,4'-oxydianiline), amic acid solution, 12.8 wt. % in 80% NMP/20% aromatic hydrocarbon) was mixed with N-Methyl-2-pyrrolidone (NMP, Sigma-Aldrich) at a volume ratio of 1:1 to make polyimide precursor ink. Around 20 ml of polyimide ink was placed in the bottle for the pneumatic atomizer. A 250 μm sized nozzle was used. An atomising flow rate of 1100 sccm, an exhaust flow rate of 900 sccm and a sheath flow rate of 140 sccm were adopted. Samples were treated at 80 ˚C for 2 hours and then 130 ˚C for 6 hours to let precursor forming polyimide.

Making and printing of PU ink

PU pellets (Elastollan® Soft 35 A 12 P) was dried and fully dissolved in NN-Dimethylformamide (DMF, Sigma-Aldrich) at 20 wt%. Around 20 ml of the PU ink was placed in the bottle for the pneumatic

atomizer. A 250 μm sized tip was used. An atomising flow rate of 1000 sccm, an exhaust flow rate of 900 sccm and a sheath flow rate of 140 sccm were adopted. Samples were dried at 80 ˚C for 0.5 hour.

Acknowledgements

S. K.-N. is grateful for financial support from the European Research Council through an ERC Starting Grant (Grant no.ERC-2014-STG-639526, NANOGEN). Q. J. is grateful for financial support through a Marie Sklodowska Curie Fellowship, H2020-MSCA-IF-2015-702868.

References:

[1] Z. Zhang, F. Ni, Y. Dong, M. Jin, H. Liu, *Sensors Actuators, A Phys.* **2013**, *194*, 196.

[2] H. Van Hoang, J. W. Jeon, *IEEE Trans. Ind. Electron.* **2011**, *58*, 3634.

[3] E. Zabler, F. Heintz, R. Dietz, G. Gerlach, *Sensors Actuators A Phys.* **1992**, *31*, 54.

[4] Z. Wu, L. Bian, S. Chen, *Sensors Actuators, A Phys.* **2018**, *273*, 232.

[5] Z. Wu, L. Bian, S. Wang, X. Zhang, *Sensors Actuators, A Phys.* **2017**, *262*, 108.

[6] C. Ciminelli, F. Dell'Olio, C. E. Campanella, M. N. Armenise, *Adv. Opt. Photonics* **2010**, *2*, 370.

[7] A. H. Kadhim, *IEEE Trans. Instrum. Meas.* **1992**, *41*, 486.

[8] Y. Park, J. Lee, J. Bae, *IEEE Trans. Ind. Informatics* **2015**, *11*, 198.

[9] M. Kim, W. Moon, *Meas. J. Int. Meas. Confed.* **2006**, *39*, 481.

[10] M. Kim, W. Moon, E. Yoon, K. R. Lee, *Sensors Actuators, A Phys.* **2006**, *130–131*, 135.

[11] F. R. Fan, Z. Q. Tian, Z. Lin Wang, *Nano Energy* **2012**, *1*, 328.

[12] M. Chen, X. Li, L. Lin, W. Du, X. Han, J. Zhu, C. Pan, Z. L. Wang, *Adv. Funct. Mater.* **2014**, *24*, 5059.

[13] Y. Su, G. Zhu, W. Yang, J. Yang, J. Chen, Q. Jing, Z. Wu, Y. Jiang, Z. L. Wang, *ACS Nano* **2014**, *8*, 3843.

[14] Y. K. Pang, X. H. Li, M. X. Chen, C. B. Han, C. Zhang, Z. L. Wang, *ACS Appl. Mater. Interfaces* **2015**, *7*, 19076.

[15] G. Zhu, Y. S. Zhou, P. Bai, X. S. Meng, Q. Jing, J. Chen, Z. L. Wang, *Adv. Mater.* **2014**, *26*, 3788.

[16] Y. Xie, S. Wang, S. Niu, L. Lin, Q. Jing, J. Yang, Z. Wu, Z. L. Wang, *Adv. Mater.* **2014**, *26*, 6599.

[17] Z. L. Wang, *ACS Nano* **2013**, *7*, 9533.

[18] Z. L. Wang, J. Chen, L. Lin, *Energy Environ. Sci.* **2015**, *8*, 2250.

[19] S. Lee, R. Hinchet, Y. Lee, Y. Yang, Z. H. Lin, G. Ardila, L. Montès, M. Mouis, Z. L. Wang, *Adv. Funct. Mater.* **2014**, *24*, 1163.

[20] G. Zhu, J. Chen, T. Zhang, Q. Jing, Z. L. Wang, *Nat. Commun.* **2014**, *5*, 3426.

[21] S. Wang, L. Lin, Y. Xie, Q. Jing, S. Niu, Z. L. Wang, *Nano Lett.* **2013**, *13*, 2226.

[22] L. Lin, S. Wang, Y. Xie, Q. Jing, S. Niu, Y. Hu, Z. L. Wang, *Nano Lett.* **2013**, *13*, 2916.

[23] X. P. Fu, T. Z. Bu, F. Ben Xi, T. H. Cheng, C. Zhang, Z. L. Wang, *ACS Appl. Mater. Interfaces* **2017**, *9*, 32352.

[24] Z. Wu, W. Ding, Y. Dai, K. Dong, C. Wu, L. Zhang, Z. Lin, J. Cheng, Z. L. Wang, *ACS Nano* **2018**, *12*, 5726.

[25] Q. Jing, Y. Xie, G. Zhu, R. P. S. Han, Z. L. Wang, *Nat. Commun.* **2015**, *6*, 8031.

[26] Q. Jing, G. Zhu, W. Wu, P. Bai, Y. Xie, R. P. S. Han, Z. L. Wang, *Nano Energy* **2014**, *10*, 305.

[27] S. Wang, Y. Xie, S. Niu, L. Lin, Z. L. Wang, *Adv. Mater.* **2014**, *14*, 2818.

[28] Y. S. Zhou, G. Zhu, S. Niu, Y. Liu, P. Bai, Q. Jing, Z. L. Wang, *Adv. Mater.* **2014**, *26*, 1719.

[29] Y. Wu, Q. Jing, J. Chen, P. Bai, J. Bai, G. Zhu, Y. Su, Z. L. Wang, *Adv. Funct. Mater.* **2015**, DOI 10.1002/adfm.201403828.

[30] W. Shang, G. Q. Gu, F. Yang, L. Zhao, G. Cheng, Z. L. Du, Z. L. Wang, *ACS Nano* **2017**, *11*, 8796.

[31] Z. L. Wang, J. Chen, L. Lin, *Energy Environ. Sci.* **2015**, *8*, 2250.

[32] L. Lin, S. Wang, S. Niu, C. Liu, Y. Xie, Z. L. Wang, *ACS Appl. Mater. Interfaces* **2014**, *6*, 3031.

[33] C. Goth, S. Putzo, J. Franke, in *Proc. - Electron. Components Technol. Conf.*, **2011**.

[34] M. Smith, Y. S. Choi, C. Boughey, S. Kar-Narayan, *Flex. Print. Electron.* **2017**, *2*, 015004.

[35] C. Ou, A. L. Sangle, A. Datta, Q. Jing, T. Busolo, T. Chalklen, V. Narayan, S. Kar-Narayan, *ACS Appl. Mater. Interfaces* **2018**, *10*, 19580.

[36] C. S. Jones, X. Lu, M. Renn, M. Stroder, W. S. Shih, *Microelectron. Eng.* **2010**, *87*, 434.

[37] K. Wang, Y. H. Chang, C. Zhang, B. Wang, *Carbon N. Y.* **2016**, *98*, 397.

[38] P. Bai, G. Zhu, Y. Liu, J. Chen, Q. Jing, W. Yang, J. Ma, G. Zhang, Z. L. Wang, *ACS Nano* **2013**, *7*, 6361.

[39] Q. Jing, G. Zhu, P. Bai, Y. Xie, J. Chen, R. P. S. Han, Z. L. Wang, *ACS Nano* **2014**, *8*, 3836.

[40] Q. Jing, S. Kar-Narayan, *J. Phys. D. Appl. Phys.* **2018**, *51*, 303001.

Figures

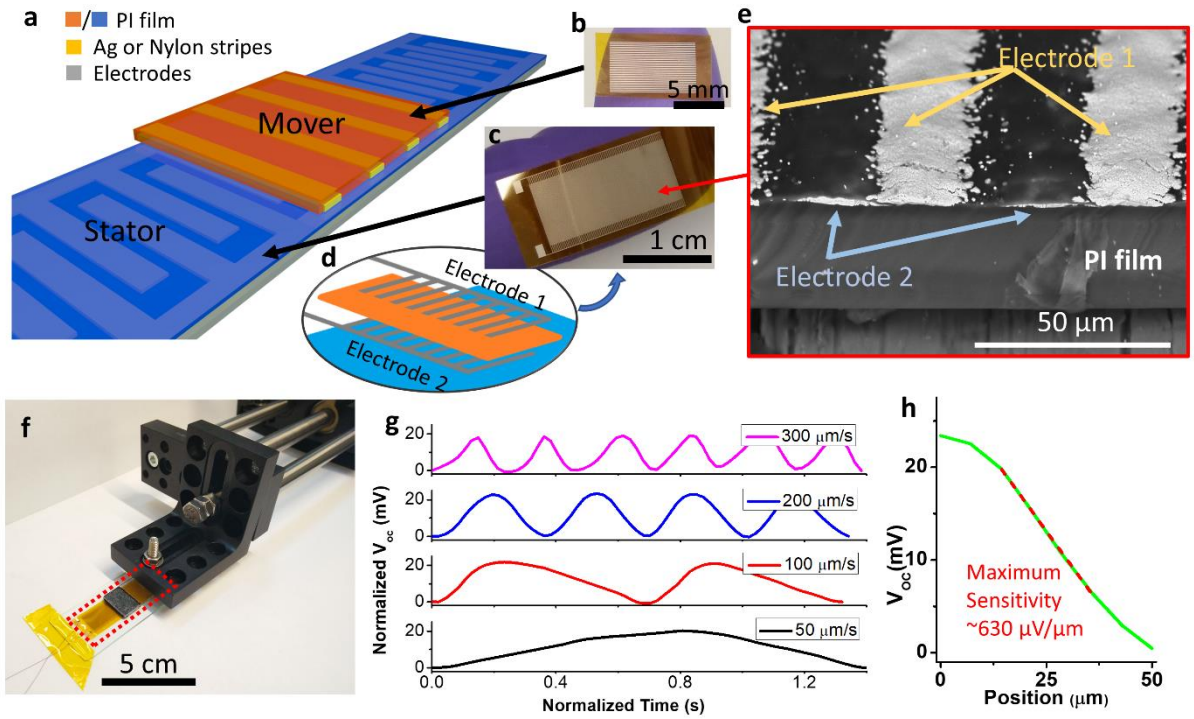

Figure 1: Triboelectric motion sensor with ultra-fine gratings. a) Schematic for free-standing grated-structure triboelectric sensor. b) Photo of the printed mover with silver on polyimide film. c) Photo of the printed stator with silver and polyimide inks on polyimide (Kapton) film substrate. The layout of the printing is illustrated in d). e) SEM image of cross-section of the stator film, showing a pair of well insulated interdigitated electrodes on the back side of the polyimide stator substrate. f) Photo showing the motion sensor being mounted on a linear motor. g) Open-circuit voltages from the sensor when working at different sliding speeds. h) Maximum sensitivity from variation of open-circuit voltage as a function of position of the mover with respect to the stator.

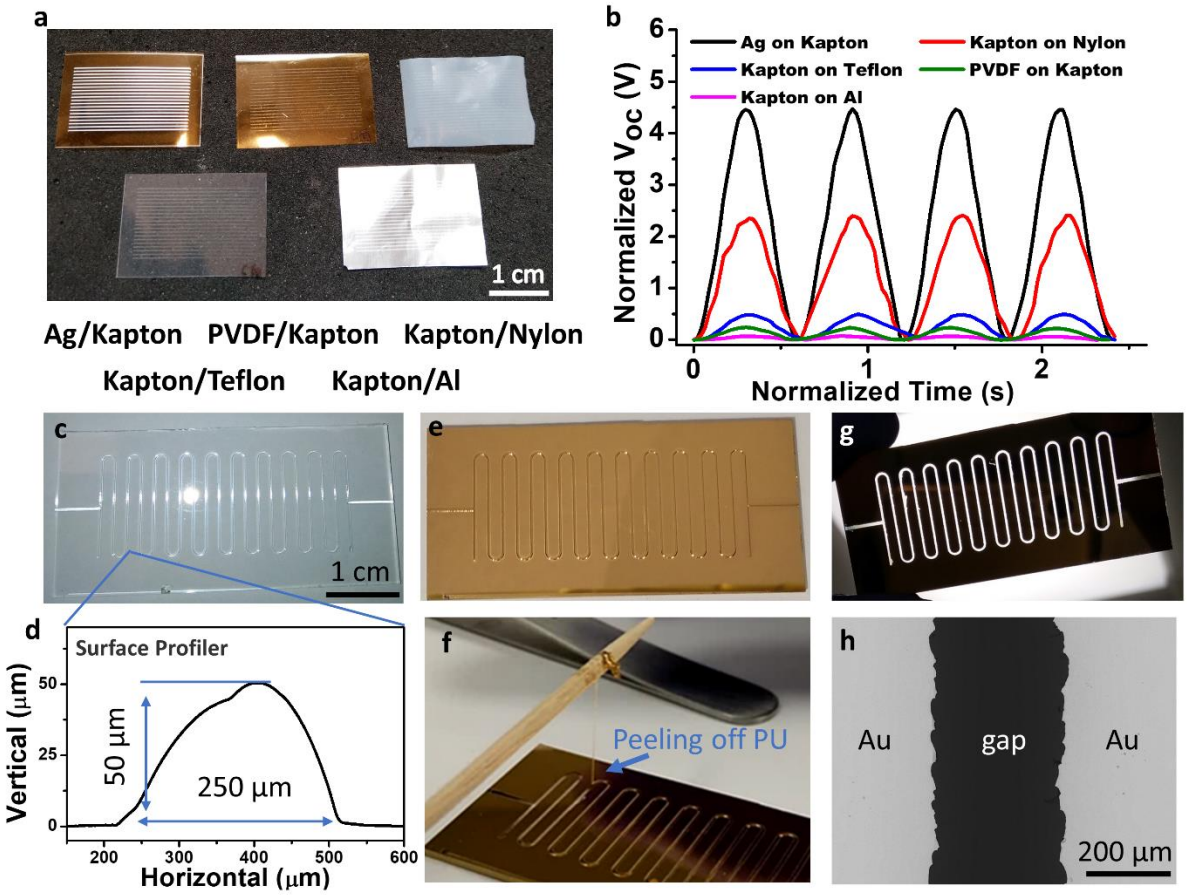

Figure 2: a) Different material inks were printed as grated structures on various substrates for comparison of output performance. b) Open-circuit voltage outputs compared from various material combinations of movers. c) Polyurethane (PU) printed as masks on glass substrate. d) Profilometer (Dektak) line scan showing the dimension of intersection of the PU masking lines. e) Gold sputtered on the masked glass substrate. f) PU directly being peeled off from the gold-coated glass, leaving interdigitated gold electrodes. g) Interdigitated electrodes observed with light source on the back. h) SEM image of edges of the gold electrodes.

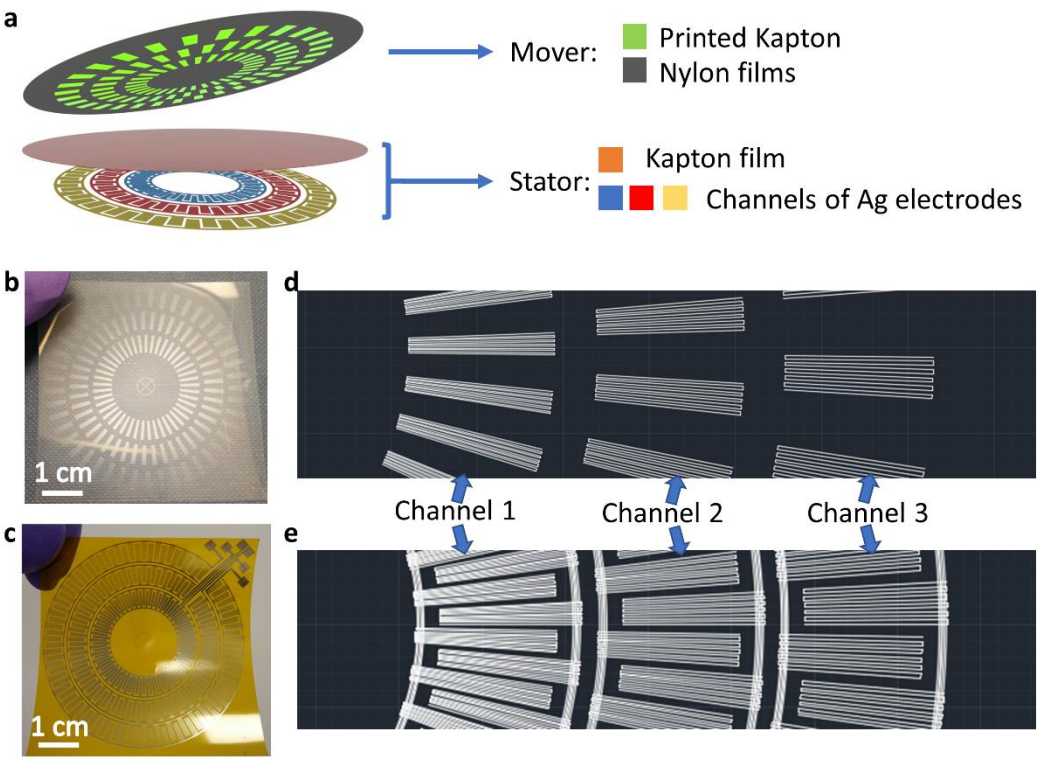

Figure 3: a) Illustration of the 3-channeled rotatory sensor. b) A photo showing the mover fabricated on Nylon film with printed radially grated polyimide. c) A photo showing the stator fabricated on polyimide film with printed silver interdigitated electrodes. d) Local CAD pattern showing the gratings on the mover possess 1/3 mismatch among each channel. e) Local CAD pattern showing the gratings on the stator are all fully aligned.

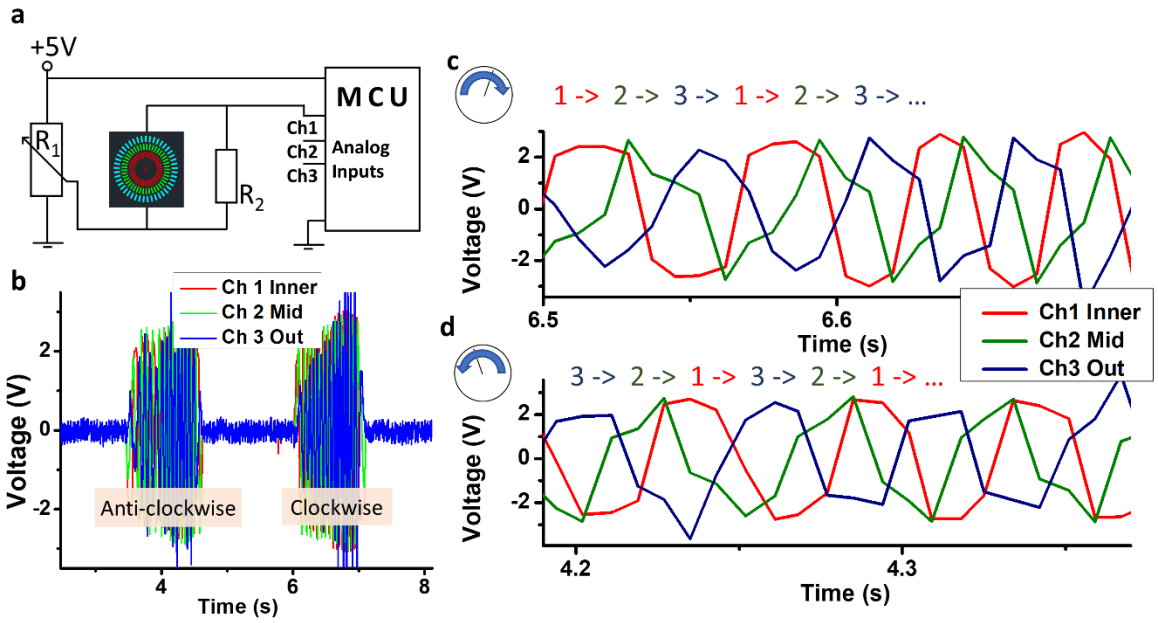

Figure 4: a) A diagram showing the processing circuit for signals generated from each channel of the triboelectric rotary sensor. b) A series of signals from three channels acquired simultaneously at both anti-clockwise and clockwise directions are displayed. c) Locally enlarged curves involving three channels of signals from clockwise rotation showing a forward order for channel 1 to 3. d) Locally enlarged curves involving three channels of signals from anti-clockwise rotation showing a reverse order for channel 3 to 1.